Supporting Information

First-Principles Study of Quaternary Thioiodides for Stable Lead-Free Solar Cells

Ming Chen,[a,b] Xiaofeng Dong,[a] Weidong Luo,[b] Zhimin Fang, [b] Zhicheng Shan,[a] Shengzhong(Frank) Liu,[b,c*] Zhuo Xu[b*]

a.School of Electric Power, Civil Engineering and Architecture, College of Physics and Electronics Engineering, State Key Laboratory of Quantum Optics and Quantum Optics Devices , Shanxi University, Taiyuan, China, 030006.

b. Key Laboratory of Applied Surface and Colloid Chemistry, National Ministry of Education, Shaanxi Engineering Lab for Advanced Energy Technology, School of Materials Science and Engineering, Shaanxi Normal University, Xi'an, China, 710119.

c. State Key Laboratory of Catalysis, Dalian National Laboratory for Clean Energy, Dalian Institute of Chemical Physics, Chinese Academy of Sciences, Dalian, China, 116023.

Computational Details

Band Gap: The DFT calculations are known to seriously underestimate the electronic band gap that is acritical quantity determining photovoltaic performance of materials. To remedy this problem, we employ the HSE hybrid functional containing the standard 25% of the exact Fock exchange to reduce the self-interaction error and reach correct gap values. The SOC effect, which plays critical role in determining electronic structures of the compounds containing heavy elements such as Bi/Pb, is included. Considering the heavy computational cost of HSE+SOC calculations for a large number of candidate compounds for materials screening, we adopt the following compromised approach: firstly we use the PBE+SOC calculations (in dense enough k-point meshes, with grid spacing of $2\pi\times0.01$ $Å^{-1}$ or less) to determine the k-points at which the band-edge states lie. Then, such k-points are passed to the HSE+SOC calculations (in moderate k-point meshes, with grid spacing of about $2\pi\times0.03$ $Å^{-1}$) from which the gap values are obtained. The assumption here is the HSE calculations do not make change to the band structure shape from the DFT-PBE calculations, which has been demonstrated to be the case in most of materials. The good agreements of gap values between theory and experiment further validate the above approach. After obtaining the band gaps from the HSE+SOC, the band structure, (projected) density of states, and absorption spectrum from the PBE+SOC calculations are corrected by the scissor operator to match the corresponding HSE+SOC gap values.

Carriers Effective Masses: We employ the semi-classical Boltzmann transport theory3 to process band structure for getting the effective mass tensors that relate directly to electrical conductivity. In this way the effects of band non-parabolicity, anisotropy of bands, multiple bands coupling, etc. on carrier transport are synthetically

taken into account. We perform the PBE calculations at the more dense k-points grid (of 2×0.005 $Å^{-1}$) to guarantee the convergence of such transport related calculations. The room-temperature mass values corresponding to the carrier concentration of 1.0x1018 cm^{-3} are taken into.

Exciton binding energy: To probe the feasibility of photon-induced exciton dissociation in solar cells, we calculate the exciton binding energy by adopting the hydrogen-like Wannier-Mott exciton model. The essential input parameters are m^* of electron and hole, and dielectric constant. Particularly, the E_b is given by $E_b=\mu^*R_y/m_0\varepsilon_r^2$, where μ^* is the reduced exciton mass (i.e. $1/\mu^*=1/m_e+1/m_h$), R_y is the atomic Rydberg energy, and ε_r is the relative dielectric constant. The high-frequency limit of dielectric constant (ε_∞) caused by electronic polarization, is taken as ε_r; the resulted E_b describes the excitons generated immediately after photon excitation (without lattice polarization process involved).

Absorption spectrum: The photon energy (ω) dependent absorption coefficient α(ω) is calculated in terms of the following relation,

$$\alpha(\omega) = \sqrt{2}\omega\left[\frac{\sqrt{\varepsilon_1^2+\varepsilon_2^2}-\varepsilon_1}{2}\right]^{\frac{1}{2}}$$

where $\varepsilon_1(\omega)$ and $\varepsilon_2(\omega)$ are real and imaginary parts of dielectric function. The $\varepsilon_2(\omega)$ is calculated in the random phase approximation[1], and $\varepsilon_1(\omega)$ is evaluated from $\varepsilon_2(\omega)$ via the Kramers-Kronig relation. The dense k-point meshes with grid spacing of 2×2×2 $Å^{-1}$ or less is used for calculating conduction and valence band states to ensure $\varepsilon_2(\omega)$ converged. The number of empty conduction band states used for such calculations is twice of the number of valence bands.

Spectroscopic limited maximum efficiency: The maximum solar cell efficiency is simulated through calculating spectroscopic limited maximum efficiency (SLME) based on the improved Shockley-Queisser model. The SLME of a material takes into account the band gap size, the band gap type (direct versus indirect), and the optical absorption spectrum, all of which can be obtained from reliable first principles calculations. The calculation of radiative and non-radiative recombination current is based on detailed balance theory using the energy difference between the minimum band gap and direct-allowed gap as the input. The detailed calculation procedure was described elsewhere.[2,3] The simulation is performed under the standard AM1.5G solar spectrum at room temperature.

Chemical bonding: For chemical bonding analyses, we utilized the COHP method as calculated by the LOBSTER package [4,5] which reconstructs the orbital-resolved electronic structure via projection of the PAW wave functions onto atomic-like basis functions. During the projection, basis sets given by Koga[6,7]were used with additional functions fitted to atomic VASP GGA-PBE wave functions. Mulliken[8,9] and Löwdin[10] population analyses from plane waves were implemented in the LOBSTER

3.0 package as briefly reviewed here.

Decomposition path: To testify the stability of these studied systems, we also calculate the decomposition energy (ΔH) according to the corresponding ternary phase decomposition pathways. The following decomposition paths of six possible photovoltaic materials are also listed in

$Sn_2SbS_2I_3$

$Sn_2SbS_2I_3 \rightarrow Sn_2SI_2 + 1/3Sb_2S_3 + 1/3SbI_3$ (1)

$Sn_2SbS_2I_3 \rightarrow SbSI + SnS + SnI_2$ (2)

$Sn_2SbS_2I_3 \rightarrow 1/4SnSb_4S_7 + 3/2SnI_2 + 1/4SnS$ (3)

$Cd_2SbS_2I_3$

$Cd_2SbS_2I_3 \rightarrow SbSI + CdS + CdI_2$ (4)

$Sn_2BiS_2I_3$

$Sn_2BiS_2I_3 \rightarrow Sn_2SI_2 + 1/3Bi_2S_3 + 1/3BiI_3$ (5)

$Sn_2InS_2I_3$

$Sn_2InS_2I_3 \rightarrow Sn_2SI_2 + 1/3InI_3 + 1/3In_2S_3$ (6)

Table S1. The calculated lattice constants using PBE schemes and computed Band gaps

(eV) for the quaternary thioiodides $M_2^{2+}M^{3+}S_2I_3$ (M^{2+} = Ca, Sr, Ba, Sn, Zn, Cd; M^{3+} = Sb) using the PBE, PBE+SOC, and HSE06 + SOC schemes. I in bracket denotes that it belong to indirect band gap, and D in brackets denotes that it belong to direct band gap.

	Material	Lattice constant (Å)			Bandgap (eV)		
		a	*b*	*c*	PBE	PBE+SOC	HSE06+SOC
Sb	$Ca_2SbS_2I_3$	4.34	15.4	16.52	1.00 (I)	0.91 (I)	1.52 (I)
	$Sr_2SbS_2I_3$	4.51	15.97	16.84	0.92 (I)	0.85 (I)	1.47 (I)
	$Ba_2SbS_2I_3$	4.71	18.37	16.38	0.94 (I)	0.86 (I)	1.49 (I)
	$Sn_2SbS_2I_3$	4.33	14.56	16.71	0.71 (D)	0.59 (D)	1.26 (D)
	$Zn_2SbS_2I_3$	4.03	15.34	16.78	2.01 (I)	1.83 (I)	2.66 (I)
	$Cd_2SbS_2I_3$	4.15	15.032	16.79	1.00 (I)	0.91 (D)	1.52 (D)

Table S2. The calculated lattice constants using PBE schemes and computed Band gaps

(eV) for the quaternary thioiodides $M_2^{2+}M^{3+}S_2I_3$ (M^{2+} = Ca, Sr, Sn, Cd; M^{3+} = Bi) using the PBE, PBE+SOC, and HSE06 + SOC schemes. I in bracket denotes that it belong to indirect band gap, and D in brackets denotes that it belong to direct band gap.

	Material	Lattice constant (Å)			Bandgap (eV)		
		a	*b*	*c*	PBE	PBE+SOC	HSE06+SOC
Bi	$Ca_2BiS_2I_3$	4.34	15.39913	16.52	1.49 (I)	1.00 (I)	1.60 (I)
	$Sr_2BiS_2I_3$	4.51	15.97	16.84	1.32 (I)	0.91 (I)	1.58 (I)
	$Sn_2BiS_2I_3$	4.33	14.58	16.50	0.71 (D)	0.36 (D)	1.09 (D)
	$Cd_2BiS_2I_3$	4.16	15.03	16.78	1.47 (I)	1.09 (D)	1.74 (D)

Table S3. The calculated lattice constants using PBE schemes and computed Band

gaps (eV) for the quaternary thioiodides $M_2^{2+}M^{3+}S_2I_3$ (M^{2+} = Ca, Sr, Ba, Sn, Cd; M^{3+} = In) using the PBE, PBE+SOC, and HSE06 + SOC schemes. I in bracket denotes that it belong to indirect band gap, and D in brackets denotes that it belong to direct band gap.

	Material	Lattice constant (Å)			Bandgap (eV)					
		a	*b*	*c*	PBE		PBE+SOC		HSE06+SOC	
In	$Ca_2InS_2I_3$	4.38	15.92	15.33	1.92	(D)	1.80	(D)	2.87	(D)
	$Sr_2InS_2I_3$	4.58	16.94	15.22	1.83	(D)	1.69	(D)	2.77	(D)
	$Ba_2InS_2I_3$	4.65	19.34	13.30	1.79	(D)	1.62	(D)	2.66	(D)
	$Sn_2InS_2I_3$	4.34	16.23	15.72	0.60	(I)	0.58	(D)	1.18	(D)
	$Cd_2InS_2I_3$	4.16	15.15	15.93	1.12	(D)	1.10	(D)	2.06	(D)

Table S4. The calculated dielectric constants of the quaternary thioiodides $M_2^{2+}M^{3+}S_2I_3$ (M^{2+} = Ca, Sr, Ba, Sn, Zn, Cd; M^{3+} = Sb) including the electron contribution (ε_∞) and the ionic contribution (ε_0); the effective masses of an electron (m^*_e)in the conduction band and a hole (m^*_h) in the valence band and exciton binding energies E_b (meV) in different directions.

Materials	Direction	Dielectric Constants			Effective Mass		Exciton Binding Energies
	k	ε_∞	ε_0	ε_{std}	m_e	m_h	E_b
$Ca_2SbS_2I_3$	X	7.15	133.37	140.52	0.33	1.96	75.14
	Y	5.68	2.51	8.19	0.24	1.34	85.80
	Z	5.97	19.08	25.05	14.30	0.52	191.46
$Sr_2SbS_2I_3$	X	6.38	66.44	72.82	0.42	1.23	104.61
	Y	4.71	2.11	6.82	0.34	5.63	196.57
	Z	5.60	17.86	23.46	9.28	0.55	225.17
$Ba_2SbS_2I_3$	X	5.79	17.01	22.8	5.20	1.42	452.50
	Y	3.75	2.05	5.8	0.91	5.79	760.54
	Z	5.27	14.49	19.76	5.20	0.65	282.93
$Sn_2SbS_2I_3$	X	11.26	49.02	60.28	0.18	0.62	14.96
	Y	8.43	13.84	22.27	0.28	0.95	41.39
	Z	8.8	11.36	20.16	0.74	2.47	100.00
$Zn_2SbS_2I_3$	X	7.92	19.73	27.65	0.46	5.08	91.45
	Y	5.28	2.98	8.26	1.46	1.64	376.80
	Z	6.01	4.43	10.44	5.19	0.54	184.16
$Cd_2SbS_2I_3$	X	9.46	33.88	43.34	0.29	15.45	43.26
	Y	7.78	7.30	15.08	0.38	0.64	53.57
	Z	9.34	106.11	115.45	0.72	0.29	32.23

Table S5. The calculated dielectric constants of the quaternary thioiodides $M_2^{2+}M^{3+}S_2I_3$ (M^{2+} = Ca, Sr, Sn, Cd; M^{3+} = Bi) including the electron contribution (ε_∞) and the ionic contribution (ε_0); the effective masses of an electron (m_e^*)in the conduction band and a hole (m_h^*) in the valence band and exciton binding energies E_b (meV) in different directions.

Materials	Direction	Dielectric Constants			Effective Mass		Exciton Binding Energies
	k	ε_∞	ε_0	ε_{std}	m_e	m_h	E_b
$Ca_2BiS_2I_3$	X	6.28	13.7	19.98	0.19	1.46	57.98
	Y	5.22	2.94	8.16	0.42	3.07	184.40
	Z	5.56	13.69	19.25	179.79	0.38	166.82
$Sr_2BiS_2I_3$	X	5.76	20.31	26.07	0.24	2.61	90.10
	Y	4.52	2.29	6.81	0.58	8.40	361.15
	Z	5.30	11.17	16.47	77.55	0.43	207.04
$Sn_2BiS_2I_3$	X	10.94	34.24	45.18	0.56	2.79	53.00
	Y	8.39	6.67	15.06	0.27	1.35	43.47
	Z	9.42	14.54	23.96	0.18	0.75	22.25
$Cd_2BiS_2I_3$	X	9.46	12.73	22.19	0.95	0.98	73.31
	Y	7.78	8.40	16.18	5.40	2.07	336.22
	Z	9.34	30.53	39.87	1.51	0.25	33.44

Table S6. The calculated dielectric constants of the quaternary thioiodides $M_2^{2+}M^{3+}S_2I_3$ (M^{2+} = Ca, Sr, Ba, Sn, Cd; M^{3+} = In) including the electron contribution (ε_∞) and the ionic contribution (ε_0); the effective masses of an electron (m_e^*)in the conduction band and a hole (m_h^*) in the valence band and exciton binding energies E_b (meV) in different directions.

Materials	Direction	Dielectric Constants			Effective Mass		Exciton Binding Energies
	k	ε_∞	ε_0	ε_{std}	m_e	m_h	E_b
$Ca_2InS_2I_3$	X	5.02	41.25	46.27	0.41	1.2	164.92
	Y	4.60	4.68	9.28	0.49	2.39	261.35
	Z	5.01	4.49	9.5	0.37	0.34	96.00
$Sr_2InS_2I_3$	X	4.56	16.67	21.23	0.38	0.45	134.75
	Y	4.25	8.32	12.57	0.73	2.72	433.34
	Z	4.57	4.74	9.31	0.54	2.13	280.52
$Ba_2InS_2I_3$	X	4.75	6.81	11.56	0.48	2.39	240.94
	Y	4.47	4.68	9.15	1.03	0.31	162.19
	Z	4.84	5.39	10.23	0.48	2.39	232.06
$Sn_2InS_2I_3$	X	8.99	45.70	54.69	0.39	26.83	64.69
	Y	7.99	13.19	21.18	0.50	2.34	87.76
	Z	9.71	10.73	20.44	0.25	0.37	21.52
$Cd_2InS_2I_3$	X	9.07	9.75	18.82	0.16	0.25	16.13
	Y	8.13	8.19	16.32	0.16	1.98	30.46
	Z	7.17	22.06	29.23	0.25	1.83	58.19

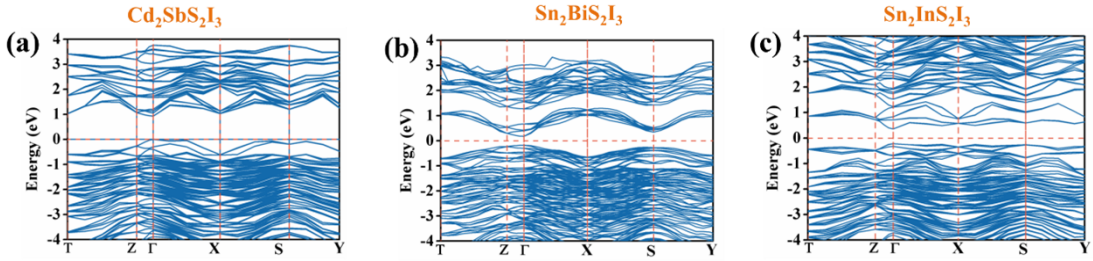

Fig. S1. Computed band structures of $Cd_2SbS_2I_3$, $Sn_2BiS_2I_3$ and $Sn_2InS_2I_3$ with PBE + SOC schemes.

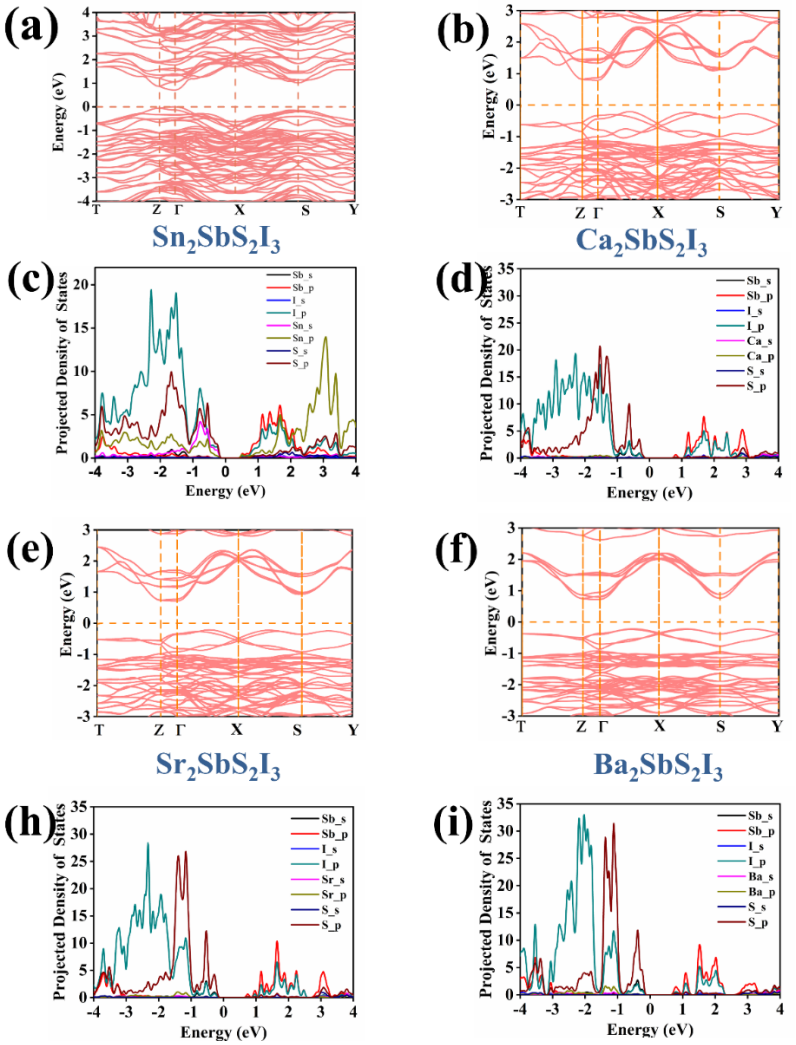

Fig. S2 Electronic band structures and projected density of states of new quaternary thioiodides based on M^{3+}= Sb: (a) and (c) belong to $Sn_2SbS_2I_3$, (b) and (d) belong to $Ca_2SbS_2I_3$, (e) and (h) belong to $Sr_2SbS_2I_3$, and. (f) and (i) belong to $Ba_2SbS_2I_3$.

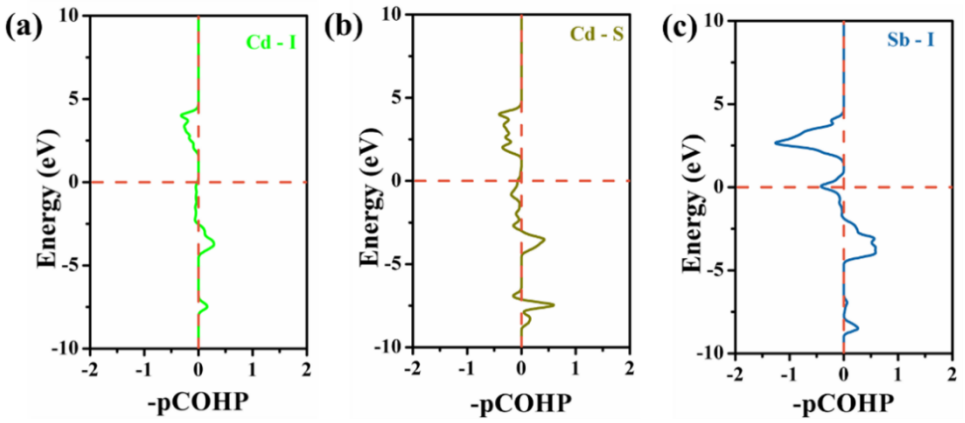

Fig. S3 The projected crystal orbital Hamilton population (pCOHP) analysis of inter (a) Sn-I (b) Sn−S and (c) Sb−I bonding interactions $Cd_2SbS_2I_3$ based on DFT plane-wave calculations.

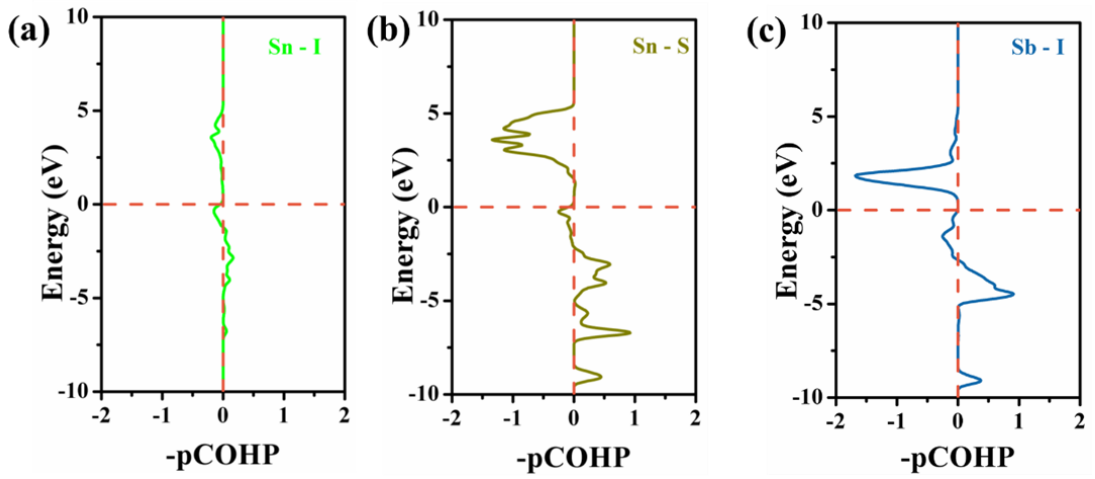

Fig. S4 The projected crystal orbital Hamilton population (pCOHP) analysis of inter (a) Sn-I (b) Sn−S and (c) Sb−I bonding interactions $Sn_2SbS_2I_3$ based on DFT plane-wave calculations.

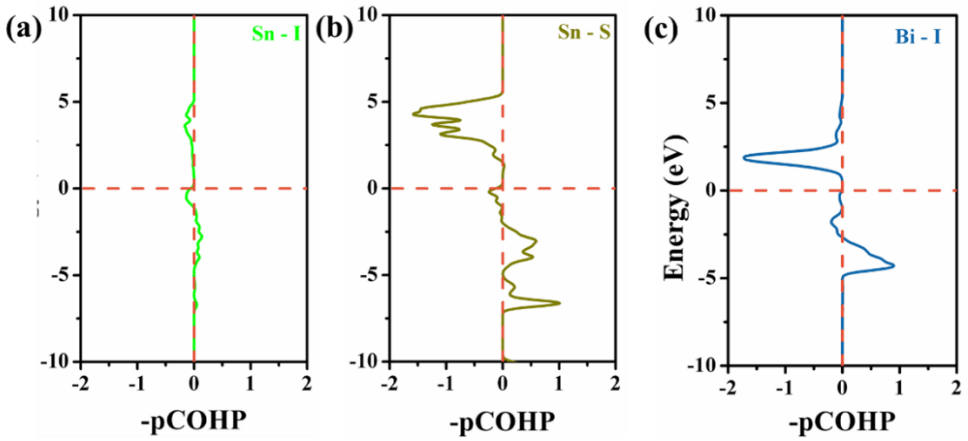

Fig. S5 The projected crystal orbital Hamilton population (pCOHP) analysis of inter (a) Sn-I (b) Sn−S and (c) Bi−I bonding interactions $Sn_2BiS_2I_3$ based on DFT plane-wave calculations.

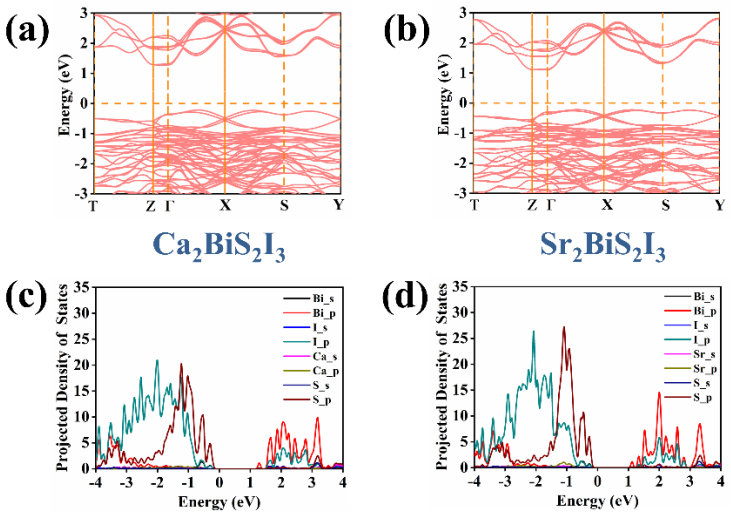

Fig. S6 Electronic band structures and projected density of states of new quaternary Thioiodides based on M^{3+}= Bi: (a) and (c) belong to $Ca_2BiS_2I_3$, and (b) and (d) belong to $Sr_2BiS_2I_3$.

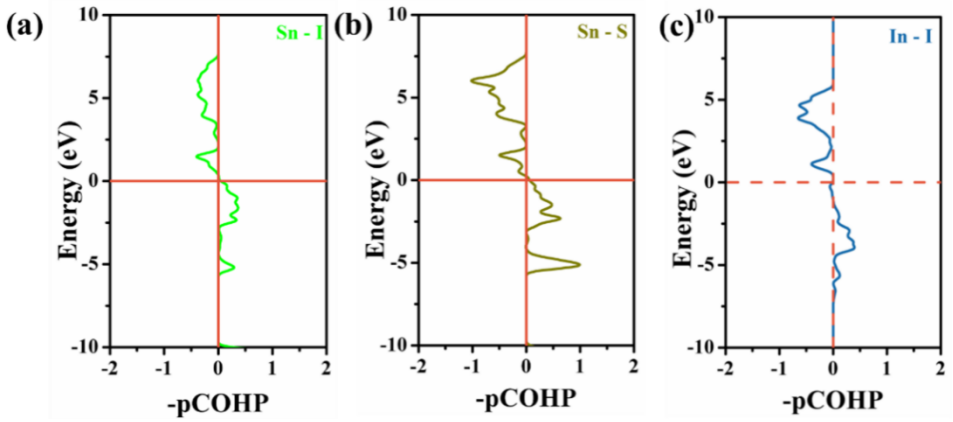

Fig. S7 The projected crystal orbital Hamilton population (pCOHP) analysis of inter (a) Sn -I (b) Sn−S and (c) In−I bonding interactions $Sn_2InS_2I_3$ based on DFT plane-wave calculations.

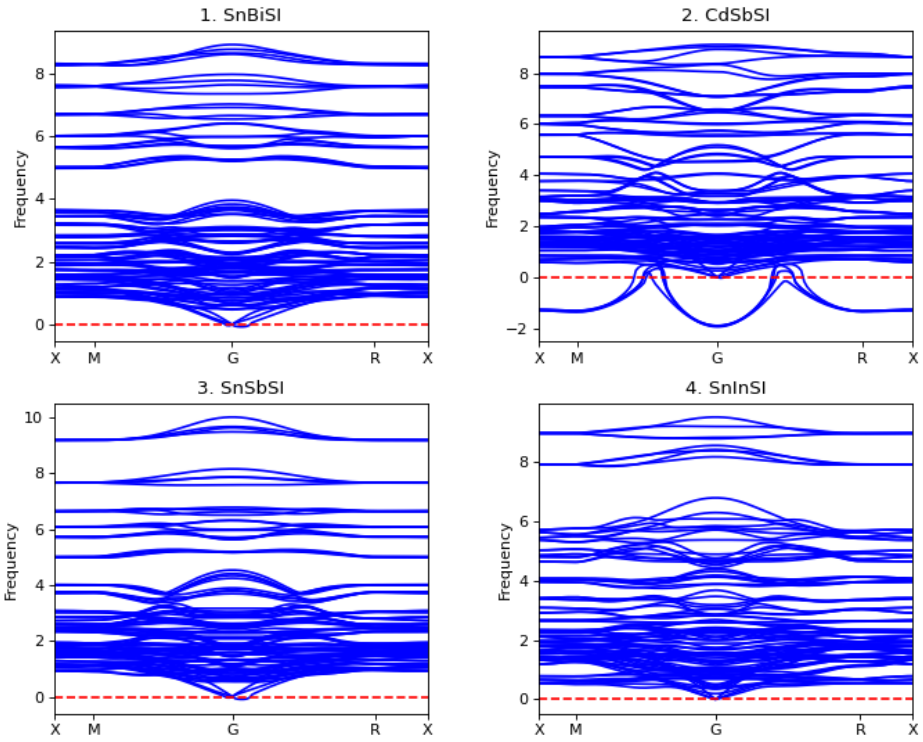

Fig. S8 Phonon dispersions of $Sn_2SbS_2I_3$, $Cd_2SbS_2I_3$, $Sn_2BiS_2I_3$, and $Sn_2InS_2I_3$.

Reference

[1] M. Gajdoš, K. Hummer, G. Kresse, J. Furthmüller, and F. Bechstedt, Phys. Rev. B. , 2006, **73**, 045112.

[2] L. Yu, A. Zunger, Phys. Rev. Lett. , 2012, **108**, 068701.

[3] L. Yu, R. S. Kokenyesi, D. A. Keszler and A. Zunger, Adv. Energy Mater. , 2013, **3**, 43–48.

[4] S. Maintz, V. L. Deringer, A. L. Tchougréeff and R. Dronskowski, J. Comput. Chem. , 2013, **34**, 2557–2567.

[5] S. Maintz, V. L. Deringer, A. L. Tchougréeff and R. Dronskowski, J. Comput. Chem. , 2016, **37**, 1030–1035.

[6] For Z=1 to Z=36: T. Koga, K. Kanayama, S. Watanabe and A. J. Thakkar, Int. J. Quantum, Chem. , 1999, **71**, 491–497.

[7] For Z = 37 to Z = 86: T. Koga, K. Kanayama, T. Watanabe, T. Imai and A. J. Thakkar, Theor. Chem. Acc. , 2000, **104**, 411–413

[8] R. S. Mulliken, J. Chem. Phys. , 1955, **23**, 1833−1840.

[9] J . Baker, Theor. Chim. Acta. , 1985, **68**, 221−229.

[10] P. O. Löwdin, J. Chem. Phys. , 1950, **18**, 365−375.